Geometric analysis of the null screens used for testing convex optical surfaces

L. Carmona-Paredes
Coordinación de Ing. Mecánica, Térmica y Fluidos, Instituto de Ingeniería,
Universidad Nacional Autónoma de México, México, D.F. 04510,
e-mail: lcp@pumas.ii.unam.mx

R. Díaz-Uribe
Laboratorio de Óptica Aplicada, Centro de Ciencias Aplicadas y Desarrollo Tecnológico,
Universidad Nacional Autónoma de México, México, D.F. 04510,
e-mail: rufino.diaz@ccadet.unam.mx

Recibido el 20 de junio de 2007; aceptado el 30 de julio de 2007

A geometric analysis of the screens used for testing convex optical surfaces is presented. Some properties of the transformation between the image plane and the screen plane, such as symmetry and magnification, are presented for the case when the reflecting surface is a sphere. Due to the intrinsic variations in the magnification, the geometric relationship between the image and the object shows some unexpected behavior. Two cases are analyzed in detail: i) a set of concentric circles centered on the origin of coordinates of the image plane with a set of radial straight lines; and ii) a square grid and a square array of circles of the same size.

Keywords: Null screens; convex optical surfaces; testing of optical surfaces.

Se presenta un análisis geométrico de las pantallas utilizadas para probar superficies ópticas convexas. Para el caso en el que la superficie reflectora es una esfera, se hace una revisión de algunas propiedades de la transformación entre el plano de la imagen y el plano de la pantalla, tales como la simetría y la amplificación. Debido a la variación intrínseca de la amplificación, la relación geométrica entre la imagen y el objeto muestra características inesperadas. Se analizan dos casos en detalle: i) un conjunto de círculos concéntricos centrados en el origen de coordenadas del plano de la imagen con un conjunto de líneas radiales; y ii) una malla cuadrada y un arreglo cuadrado de círculos del mismo tamaño.

Descriptores: Pantallas nulas; superficies ópticas convexas; pruebas ópticas.

PACS: 42.15.-i; 42.30.-d; 42.62.Eh; 42.87.-d

1. Introduction

The testing of optical surfaces using null screens is based on the analysis of the image of a cylindrical screen with a set of curves drawn on it in such a way that its image, which is produced by reflection on the test surface, yields a pattern previously determined [1]. The screen, made of a sheet of paper which hereafter will be called the "plane screen" or simply the "*screen*", is rolled up to make a cylindrical screen. The test surface is placed inside the cylinder and is illuminated from outside by white light; the light rays transmitted to the inside of the cylinder are reflected on the test surface, collected by a lens, passed through a pinhole, and the image is captured with a CCD camera (Fig. 1). The CCD sensor is in the image plane.

A qualitative test of the optical surface consists of checking that the image of the cylindrical screen, defined previously, is the same as the design image. Usually, the image of the cylindrical screen is chosen to be a simple geometric array such as a perfect square grid, concentric circles or straight lines, in order to detect easily, with the naked eye, any departure from the prescribed geometry. For simplicity, through out this paper the cylindrical screen will be called the "*cylinder*" or "*screen*" and the image screen the "*image*".

To test quantitatively the optical surface, it is necessary to associate a point of the image with its corresponding point in the cylinder to obtain the normal vector to the test surface at each point of incidence. After a numerical integration method, the sagitta of the test surface is obtained. Then, it is possible to compare the sagittas of an ideal surface with those of the test surface [2]. A problem in calculating the normal vectors to the test surface is that on the image there are no single, isolated points; instead, there are finite sized spots. Thus, the geometric centroids of the spots are usually assigned as the points on the image to obtain the sagittas.

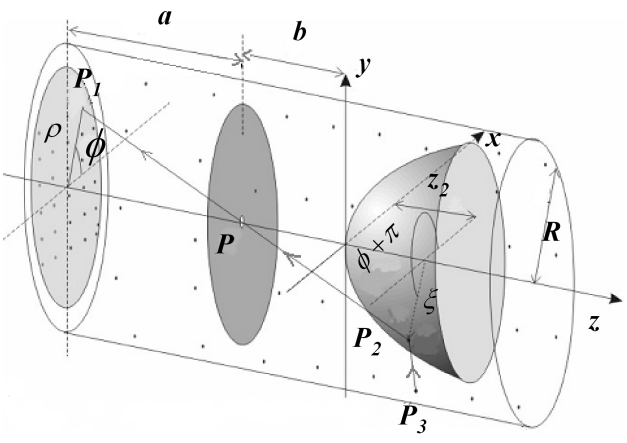

FIGURE 1. Optical setup for testing convex surfaces with the null screen.

The goal of this paper, for a better understanding of the relationship between the image and the screen is to show, particular characteristics of some types of curves on the image and their corresponding curves on the screen for the case when the surface is a sphere. In addition, it will be shown that the positions of geometric elements of the curves on the image do not always correspond to the same geometric positions on the screen. The results obtained here can be easily extended to any other convex and conic optical surfaces.

In Sec. 2, the transformation function that relates the coordinates of the points on the image to the coordinates of the points on the cylinder, as well as other useful definitions are presented. Some simple arrays of curves on the image as a square grid and a square array of circles of the same size, is presented in Sec. 3; in this section, it is also shown, through a particular example, that it is possible to obtain the screen of any picture on the image. In Sec. 4, the magnification of the image, defined as the size ratio of a segment on the image to the corresponding one on the screen, is analyzed. The conservation of symmetry of the transformation function is analyzed in Sec. 5. Finally, in Sec. 6, comments and conclusions are presented.

2. Transformation from the image to the screen

In order to introduce the transformation between the points on the image and the points on the cylinder, it is important to see how the image is produced. From the bundle of rays scattered from a point P_3 (see Fig. 1) on the cylinder, only one ray strikes the optical surface (point P_2); it is reflected and then passes through the pinhole P. Finally, this ray impinges on the CCD to form the image (P_1) of the point P_3. As this happens for every point on the cylinder, an image of the cylinder is formed at the CCD.

For each point on the image, the positions of the corresponding points on the cylinder are obtained with the reverse ray calculation method proposed in Ref. 1, $i.e.$ opposite to the actual ray propagation direction. Unless otherwise stated, this will be the ray direction analyzed throughout this paper. In Ref. 1, the transformation is developed for any conical optical surface; in the present paper, only the spherical case will be considered.

Due to the symmetry of revolution of the problem, Fig. 1, it is better to use cylindrical coordinates to describe the curves on the cylinder and on the image. So, in reference to Fig. 1, $P_1 = (\rho, \phi, -a-b)$, $P_2 = (\xi, \phi+\pi, z_2)$ and $P_3 = (R, \phi+\pi, z_3)$.

The transformation is given by the following equations:

$$\xi = \frac{a(b+r) - (a^2r^2 - \rho^2 b(b+2r))^{1/2}}{a^2+\rho^2}\rho \qquad (1)$$

$$z_2 = \frac{\xi}{\rho}a - b. \qquad (2)$$

and

$$z_3 = \frac{Ua - V\rho}{U\rho + Va}(\xi - R) + z_2; \qquad (3)$$

where

$$U = \xi^2 - W^2, \quad V = 2\xi W \quad \text{and} \quad W = z_2 - r. \qquad (4)$$

In the last equations, R and r are the radii of the cylinder and spherical surface, respectively.

The relationship between the cartesian coordinates (X, Y) on the screen and the cylindrical coordinates (R, ϕ, z_3) on the cylinder is given by:

$$X = R\phi \qquad (5)$$

and

$$Y = z_3(\rho). \qquad (6)$$

To design real screens, it is important to know the transformation range. So, for the angular coordinate, it is clear from Eq. (5) that X is a linear function of ϕ and is defined for all values of ϕ. Even though X and ϕ are defined for all values, they can be considered to be restricted by

$$0 \leq \phi \leq 2\pi \qquad (7)$$

and

$$0 \leq X \leq 2\pi R. \qquad (8)$$

For the radial coordinate, in order to have only real numbers of the coordinate Y, ρ must satisfy

$$\rho \leq \frac{ar}{[b(b+2r)]^{1/2}}. \qquad (9)$$

From Eqs. (1) and (2) it can be seen that, if ρ tends to zero, then ξ and z_2 tend to zero, and from Eqs. (3) and (6) it is obtained that $z_3 \to -\infty$. Thus, as ρ tends to zero, the length of the screen tends to be very large. The points with very small ρ correspond to the images of the points near the reflecting surface vertex. The limit ρ = 0 corresponds to the image of the reflecting surface vertex (see Fig. 1) so, in order to see the image of the sphere vertex, the screen must be indefinitely long. Since it is not possible to construct such a screen, the origin of the image coordinate system is always absent from the image, and $\rho > 0$.

In order to have some insight into the behavior of the radial coordinate of the transformation, Eq. (6) is plotted in Fig. 2 for a particular case. It can be seen that for small values of ρ, Y grows very fast; as $\rho > 0.5$ approximately, it begins to grow slower. For values of ρ such that Y is near zero, the transformation is almost linear. For larger values of ρ, Y starts to grow faster.

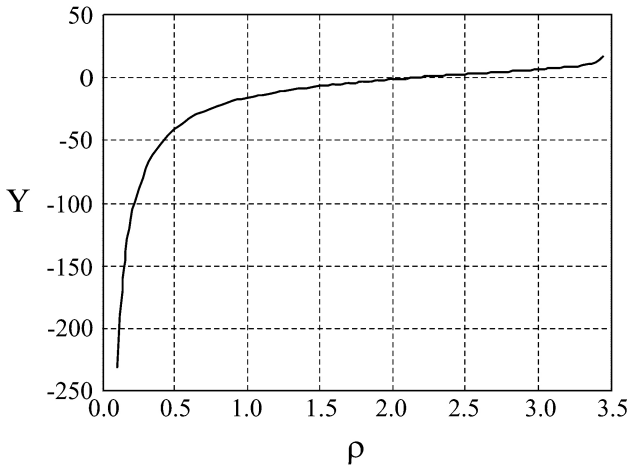

FIGURE 2. Plot of the transformation from the image to the plane screen.

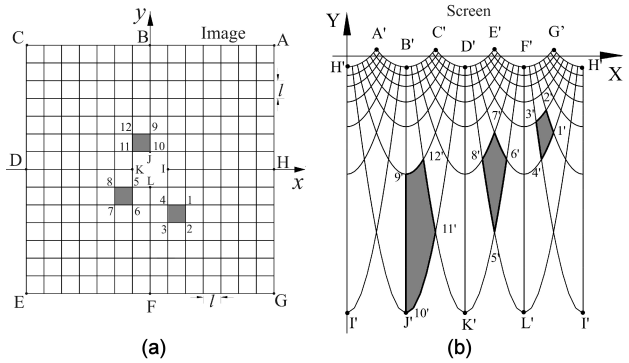

FIGURE 3. (a) Square grid on the image. (b). *Trapezoids* on the screen.

3. Some simple patterns on the image

In order to use the null screen method to test optical surfaces, it is best to observe images formed by very simple patterns in such a way that it is easy to detect any difference between the images formed by the real surface and those that were designed. So, in the following sections, two simple patterns on the image are presented.

3.1. Square grid

In order to test qualitatively an optical surface, one of the most useful and simple patterns for the image is a square grid (see Ref. 1). This pattern (Fig. 3a) is obtained on the image when the plane screen is designed with a set of curves that appear as shown in Fig. 3b. Since the objects on Fig. 3b are like trapezoids with curved sides, they will be called simply *trapezoids*.

The square grid on the image is formed with vertical and horizontal lines with equations

$$x = nl \quad \text{and} \quad y = ml, \tag{10}$$

respectively, where n, m = 0, ±1, ±2, ...,$\pm N$, *Nl = d*/2; d is the length side of the smallest side of the CCD (for more details see Ref. 1).

The points on the image that satisfy both Eqs. (10) at the same time are the crossing points between the horizontal and vertical lines. On the plane screen, it is not enough to plot only the corresponding crossing points, it is better to find the position of several points; between the crossing points. Ten equally-spaced points are adequate. Along the horizontal direction, the coordinates of the ten equally-spaced points between the crossing points (x_n, y_m) and (x_{n+1}, y_m) are

$$x_{n_j} = nl + \frac{jl}{10} \quad \text{and} \quad y_m = ml, \tag{11}$$

where m=0, ±1,...,$\pm\boldsymbol{N}$, n=0, ±1,...,$\pm N-1$ and for each value of n, j=0,...,10.

For the vertical direction, the coordinates of the ten points between the crossing points (x_n, y_m) and (x_n, y_{m+1}) are

$$y_{m_k} = ml + \frac{kl}{10} \quad \text{and} \quad x_n = \boldsymbol{nl} \tag{12}$$

where n=0, ±1,...,$\pm N$, m=0, ±1,...,$\pm N-1$ and for each value of m,k=0,...,10.

In order to plot the plane screen, Eqs. (5) and (6) are applied to the polar coordinates of the points given by Eqs. (11) and (12), $i.e.$ they are applied to:

$$\phi = \tan^{-1}\left(\frac{m}{n+j/10}\right) \rho = \left[\left(n+\frac{j}{10}\right)^2 + m^2\right]^{1/2} l, \tag{13}$$

and

$$\phi = \tan^{-1}\left(\frac{m+k/10}{n}\right) \rho = \left[n^2 + \left(m+\frac{k}{10}\right)^2\right]^{1/2} l \tag{14}$$

In Fig. 3b, the calculated points are joined with straight lines.

For a better understanding of the geometry of the image and its screen in Fig. 3, some points on the image are indicated with capital letters and their corresponding points on the screen with the same prime capital letter. The points on the plane screen will be denoted by primed capital letters, and the corresponding points on the image will be written without primes.

It can be seen that the points on the image with the largest value of ρ, $i.e.$ the square grid vertex (points A, C, E and G) are transformed into the points on the screen with the largest Y values. The points on the image with the smallest values of ρ (points I, J, K and L) correspond to the points on the screen with the smallest values of Y. It is interesting to note that the straight lines defined by the pairs of points *IH*, *JB*, *KD* and *LF* are the only ones that are transformed on the screen into straight lines; any other straight line on the image is seen on the screen as a curve. This result is due to the fact that, in the image, these are radial lines.

In addition, on the same image, Fig. 3a, three squares are marked with dark lines and their vertices are numbered in a

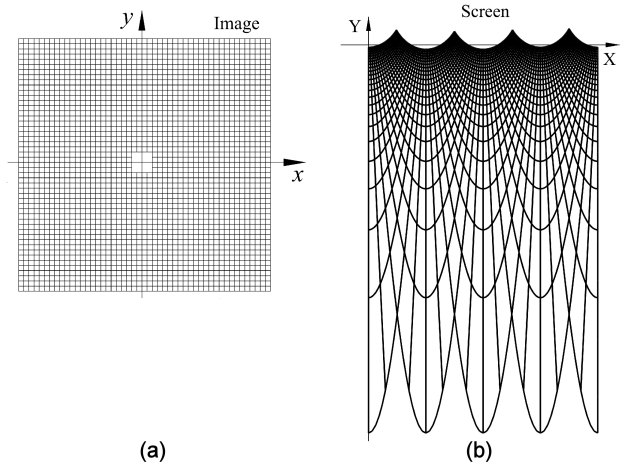

FIGURE 4. On the image, the line density is constant. (b) On the screen, at the top, the curve density is greater than at the bottom.

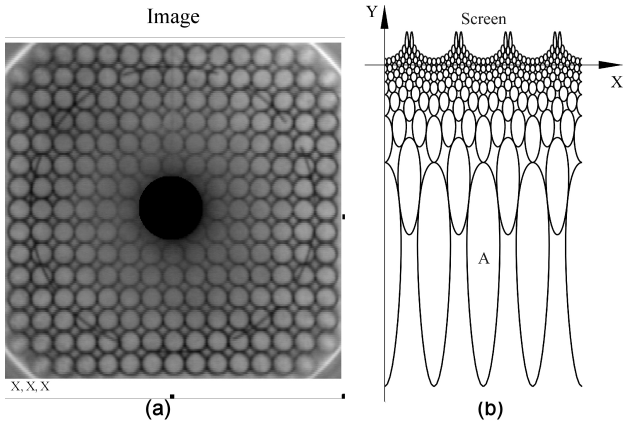

FIGURE 5. (a) Array of circles of the same size on the image. (b) Screen with curves like *drops.*

clockwise direction. On the screen, Fig. 3b, their corresponding *trapezoids* are also marked with dark lines and the vertices are numbered to maintain the correspondence between the vertices on the image and those on the screen. It is interesting to note that:

i) while the numbers of the vertices of the squares grow in the clockwise direction, on the vertexes of the *trapezoids*, they grow in the counter clockwise direction;

ii) in each square, the upper right vertex has been identified with the smallest number of the four vertices. Nevertheless, on the *trapezoids* the relative position of the vertex marked with the smallest number is not the same with respect to the other three vertexes. For instance, for one square on the image (Fig. 3a), vertex 4 is at the upper left corner and on its corresponding *trapezoid* on the screen (Fig. 3b), it is placed at the bottom. For other squares, the result is different.

The form and size of a *trapezoid* on the screen depend on the position of its corresponding square on the image. Looking carefully at Fig. 3b, it can be seen that the *trapezoids* marked with dark lines show the three kinds of *trapezoids* on the screen. The *trapezoid* with vertices 5', 6', 7' and 8' is the only one showing symmetry; it is symmetric with respect to a vertical line. The *trapezoid* with vertices 9', 10', 11' and 12' has one straight side and that one defined by the vertices 1', 2', 3' and 4' has its four sides curved and does not present any symmetry. Any other *trapezoid* on the screen is like one of these three but with a smaller dimensions, or perhaps reflected 180° with respect to a vertical line.

From Fig. 3b it can be seen that the *trapezoid* area depends mainly on the vertical position: those farthest from the X-axis have the largest area, and this decreases as they are nearer to the X axis. This fact means that, while on the image the distribution of the lines forming the squares is uniform over the area of the screen, on the plane screen, Fig. 3b, at the top, the curve density is greater than at the bottom. In Fig. 4, this effect is more clearly shown: in (a) a square grid with constant density of lines is plotted and its plane screen, which shows a clear variation of the curves density in the vertical direction, is plotted in (b). On the plane screen, the dependence on the vertical direction of the line density is a consequence of the transformation dependence on the radial coordinates [Eq. (6)].

3.2. Square array of circles on the image

The accuracy of the testing of a surface depends on the accuracy of the evaluation of the coordinates of the centroids, as discussed in Ref. 2. Many authors [5-8] have proposed different methods and techniques in order to increase the accuracy of the centroid estimation; all of them use statistical analysis on the evaluation of the centroid. Therfore, it is important to use bright spots instead of single points on the image.

The interest in analyzing an array of circles on the image comes from the idea of having images with a simple spot geometry in order to easily find the centroid of each spot. As is known, in this case the positions of the centroids coincide with the centers of the circles provided that they are evenly illuminated. In Ref. 3, it was proposed that the bright spots should become circles. The objects on the screen that produce circles on the image have oval-like forms (see Refs. 3 and 4), that will be called *drops*, because of the asymmetry that will be shown later.

A squared array of equal circles on the image is proposed, so the centers of the circles are set on a square grid and the circles radii are equal. Then, each circle is defined by the equation

$$(x - x_0)^2 + (y - y_0)^2 = r^2, \tag{15}$$

where x_0, y_0 = 0, $\pm d$, $\pm 2d$, ...,$\pm Nd$, *Nr* = *d*/2 and r is the radius of the circles.

To obtain the curves on the plane screen, the transformation (Eqs. (5) and (6)) is applied to the polar coordinates of the points given by Eq. (15).

Each circle in Fig. 5a was formed with 72 points joined with straight lines, with one point every 5°. In this case, the parameters indicated in Fig. 1 were R =15.85 mm,

$a = 20.77$ mm and b =64 mm, the test surface radius r =11.125 mm; the lens focal distance of the camera used to take the photo shown in Fig. 5a was f = 16 mm and the width of the CCD square grid, d =4.4 mm. The parameters a and b (Fig. 1) were chosen so that the diameter of the test surface fit the area of the CCD (for details see Ref. 1).

In order to observe circles of the same size on the CCD, the sizes and shapes of the *drops* must be different, depending on their position on the screen. The bottom end of each *drop* on the most negative side of the Y-axis (such as *drop* A in Fig. 5b) is narrower than its top end, while *drops* near the X-axis are more symmetric, more like ellipses. This is because the radial magnification is nearly constant around the X-axis, while far from there the magnification varies, as will be shown later.

The images of the *drops* are seen on the CCD plane as circles inscribed in an imaginary region defined by the points a, b, c and d, as is indicated by dotted lines in Fig. 6a. Each *drop* on the plane screen is inscribed in an imaginary rectangle with vertices a', b', c' and d', as shown in Fig. 6b. It is not difficult to find that, in general, the centers of the circles on the image are not transformed into the middle point of the longitudinal axis of the *drops*. In Fig. 6a, C is the center of the circle and M', the longitudinal axis middle point of the *drop* in Fig. 6b, is not its corresponding point. It is worth

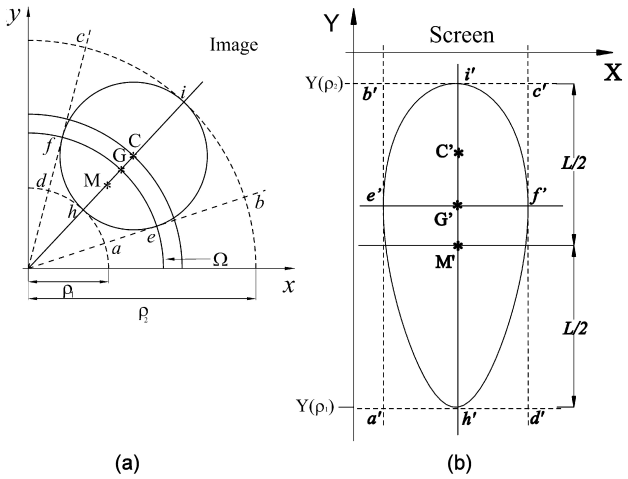

FIGURE 6. (a) Some points of interest on the image are marked. (b) The corresponding points on the screen are marked.

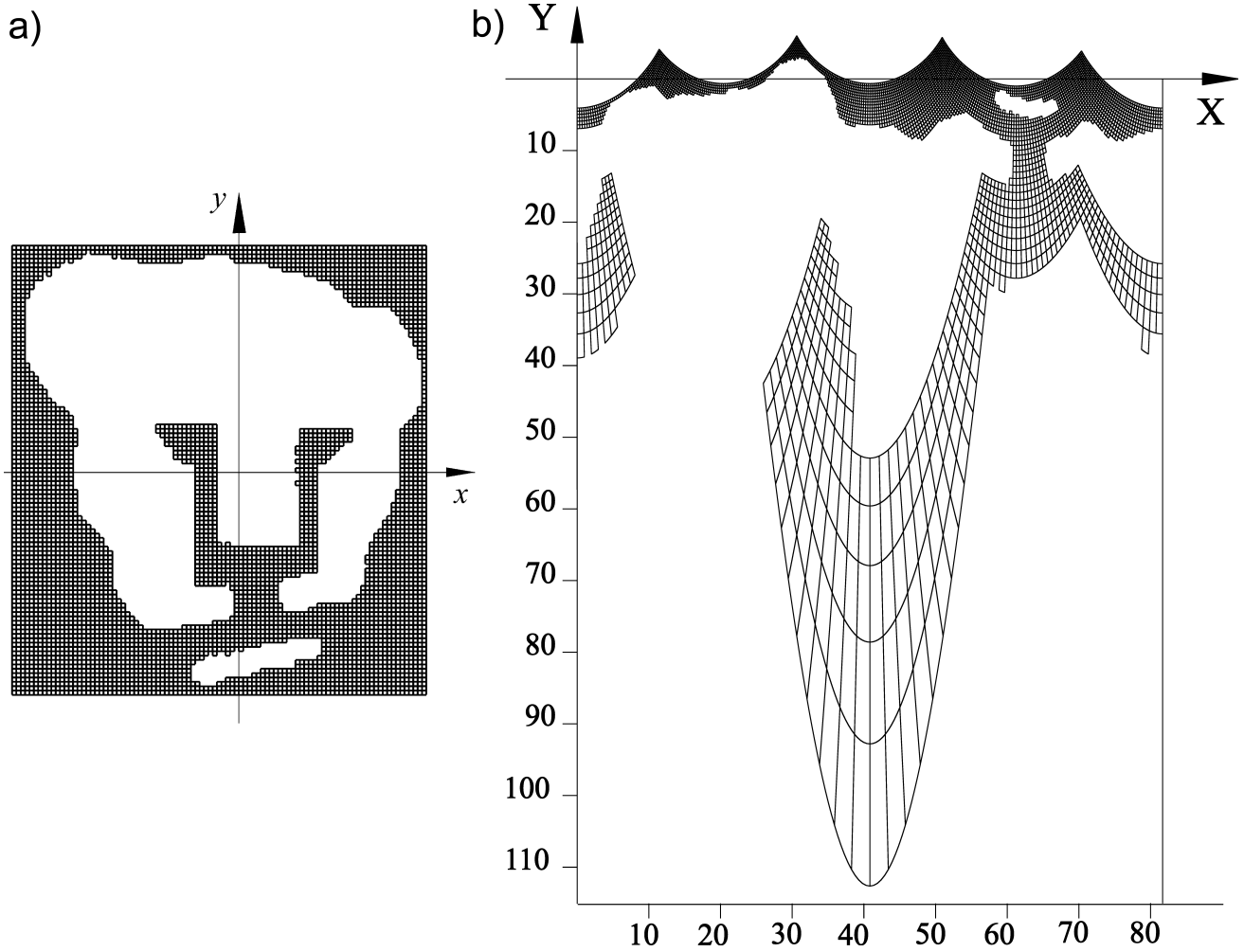

FIGURE 7. (a). Image of the "Puma" of the Universidad Nacional Autónoma de Mexico; (b). Screen which produces the "Puma" when it is reflected on a sphere with 11.125 mm of radius of curvature (a steel ball 7/8-in diameter is adequated). Dimensions in mm.

noting that the only point inside the circle (on the image) that can geometrically be easily related to its corresponding point on the *drop* (on the screen) is the point G in Fig. 6a. This point results from intersecting the circle Ω passing through points e and f (where the radial lines are tangent to the circle) and the radial line passing through C and joining the points h and i. The arc of the circle Ω is transformed, on the plane screen, into the horizontal line passing through points e' and f' (the points where the vertical lines are tangent to the *drop*), while the radial line is transformed into the vertical line passing through h' and i'. The point G' is the intersection point between these two lines. About the positions of points C and M (on the image) and their corresponding points on the screen C' and M', along the azimuthal direction, it can be said that they are on the same vertical line as the point G'. Along the radial direction, the answer is not so direct and will be discussed in Sec. 4.

3.3. Any picture on the image

In previous sections, images with very simple patterns such as lines, squares and circles were shown. However, it is possible to develop screens in order to observe any picture on the image. As an example, in this section, a stylized Puma in Fig. 7a and its screen in Fig. 7b are shown. The Puma is one of the emblems of the Universidad Nacional Autónoma de México.

Using a computer program, the coordinates of the pixel vertices and the coordinates of five points between two consecutive vertices were calculated. Note that Fig. 7a is an array of squares. The transformation is applied to the coordinates of each vertex and to the additional five points between them, in order to obtain their corresponding points on the screen. Then they are joined with straight lines to obtain the screen shown in Fig. 7b. It is important to keep the real scale while plotting a screen. To develop the screen in Fig. 7b, the optical parameters used were r = 11.125 mm, R= 13 mm, a = 30 mm and b = 86 mm.

Although the image presented in this section is black and white, it is possible to obtain screens in order to see color images. To do this, the color assigned to each pixel of the picture must be assigned to the corresponding *trapezoid* area obtained after applying the transformation.

Figure 7b can easily be used for observing the Puma image. Figure 7b should be copied to form a cylinder. Also, the discontinuous line in the figure should be aligned with the Y-axis. A steel sphere 7/8-in diameter should be introduced into the cylinder. Special care must be taken in order to ensure that the top of the sphere (vertex, see Fig. 1) is level with the X-axis in the figure; while looking inside the cylinder, it may be necessary to come closer or to move further away from the steel ball in order to bring the image into focus It is recommended that the screen be printed on paper which is not completely opaque.

4. Magnification of the image

The magnification of an image M can be defined, as in paraxial optics, as the quotient of an image segment $\overline{AB}$ divided by its corresponding object segment $\overline{A'B'}$ on the plane screen:

$$M = \frac{\overline{AB}}{\overline{A'B'}}. \tag{16}$$

It is clear that the magnification will depend on the orientation of the chosen segments. Since Eqs. (5) and (6) define the transformation in parametric form, where the parameters are ρ and ϕ, it is possible to define two basic magnifications: a radial magnification M_ρ, which relates vertical segments on the screen ΔY with radial segments $\Delta\rho$ in the image, and an azimuthal magnification M_ϕ that relates horizontal segments ΔX on the screen with arc segments $\rho\Delta\phi$ in the images (see Fig. 10).

4.1. Radial magnification

The radial magnification M_ρ is given by

$$M_\rho = \frac{\Delta\rho}{\Delta Y}. \tag{17}$$

To obtain this, the inverse of Eq. (3) must be known. This is not easy to obtain analytically, so the radial magnification is calculated through the derivative of Y with respect to ρ, and then taking their multiplicative inverse. Using Eqs. (1) to (6), the following expression is obtained:

$$\frac{dY}{d\rho} = \frac{\left[a\frac{dU}{d\rho} - \left(\rho\frac{dV}{d\rho} + V\right)\right](U\rho + Va) - (Ua - V\rho)\left[\rho\frac{dU}{d\rho} + U + a\frac{dV}{d\rho}\right]}{(U\rho + Va)^2}(\xi - R) + \frac{Ua - V\rho}{U\rho + Va}\frac{d\xi}{d\rho} + \frac{dz_2}{d\rho}, \tag{18}$$

where

$$\frac{dV}{d\rho} = 2\left(\xi\frac{dz_2}{d\rho} + W\frac{d\xi}{d\rho}\right), \tag{19}$$

$$\frac{dz_2}{d\rho} = \frac{a}{\rho^2}\left(\rho\frac{d\xi}{d\rho} - \xi\right), \tag{20}$$

and

$$\frac{d\xi}{d\rho} = \frac{\rho b\left(a^2+\rho^2\right)(b+2r)}{\left(a^2r^2 - \rho^2 b\,(b+2r)\right)^{1/2}} + \frac{\xi}{\rho}\left(1 - \frac{2\rho^2}{a^2+\rho^2}\right). \tag{21}$$

The radial magnification is plotted in Fig. 8, for the case

of R = 13 mm, r = 11.125 mm, a = 30 mm and b = 86.05 mm. It can be seen that it grows smoothly for values of ρ less than 2.6 and reaches its maximum at a value of ρ close to 2.6. For larger values of ρ, the radial magnification rapidly decreases.

4.2. Azimuthal magnification

The azimuthal magnification M_ϕ, is defined as

$$M_\phi = \frac{\rho \Delta\phi}{\Delta X}. \tag{22}$$

Substituting Eq. (5) in Eq. (22), the azimuthal magnification can be expressed in a very simple form:

$$M_\phi = \frac{\rho}{R}; \tag{23}$$

$i.e.$ along a circle of radius ρ on the image, the azimuthal magnification is constant, because it does not depend on the azimuthal angle ϕ. For Y = const, the azimuthal magnification is constant too because Y is directly related to ρ through Eq. (3). M_ϕ changes linearly with ρ, as is shown in Fig. 9.

It is quite interesting to note that the azimuthal magnification is a linear function of ρ, while the radial magnification depends implicitly on ρ.

Going back to the point of knowing the relative position in radial (on the image) and vertical (on the screen) directions between the points C, M and G in Fig. 6, it has been found that this depends on whether ρ_C (point C radial coordinate) is greater than, equal to or less than ρ_{max}(the value of ρ where the radial magnification reaches its maximum value (see Fig. 8). There are three possible cases to be analyzed.

In order to analyze these cases, consider the following definitions. On the image, let $r = \rho_i$- ρ_C=ρ_C- ρ_h be the circle radius; on the screen, $Y_H = Y_{C'} - Y_{h'}$ and $Y_I = Y_{i'} - Y_{C'}$ and the radial magnification $M_H = r/\mathrm{Y}_H$ and $M_I = r/\mathrm{Y}_I$.

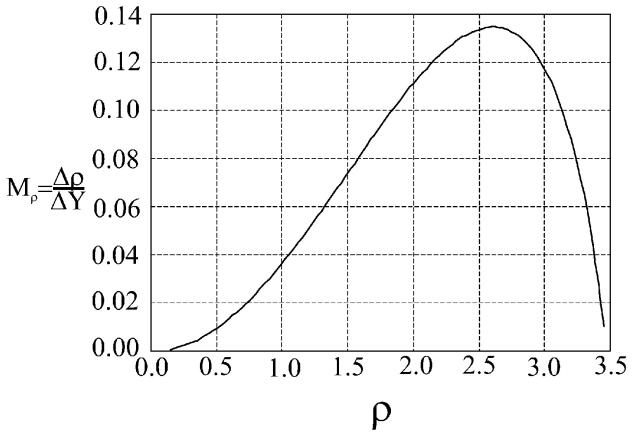

FIGURE 8. Radial magnification.

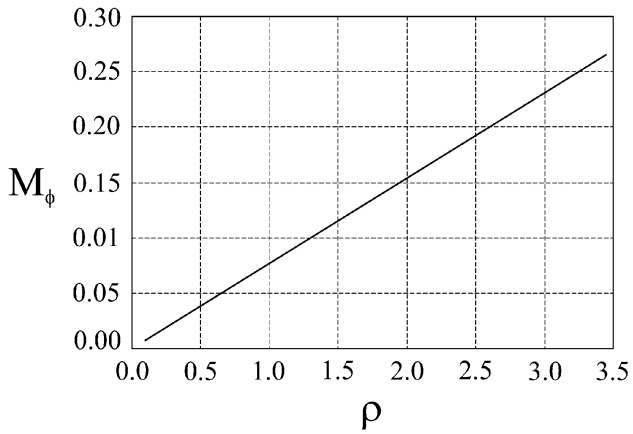

FIGURE 9. Azimuthal magnification.

Case 1. It is assumed that $\rho_h > \rho_{max.}$. In this case, the radial magnification decreasing with ρ. Since $\rho_h < \rho_C < \rho_i$, then $M_H > M_I$, so $\mathrm{Y}_H < Y_I$. This means that C' is nearer h' than i', $i.e. C'$ is below the mid-point of the *drop* M'.

Case 2. In this case, it is assumed that $\rho_i < \rho_{max}$, so that the circle in Fig. 6(a) is in the region where the radial magnification is increasing with ρ. Since $\rho_h < \rho_C < \rho_i$, then $M_H < M_I$, which implies $Y_H > Y_I$. So, on the screen, C' is farther from h' than i'. This means that C' is above the mid-point of the *drop* M'.

Case 3. In the case that $\rho_C \approx \rho_{max}$ and r is small enough so that $M_H \approx M_I$, C' coincides with M'.

On the image, when the centroid coordinates of the circular spots are calculated, it must be remembered that, in general, their values do not coincide with the geometric center coordinates of the *drop*.

5. Symmetry of the transformation

From Eqs. (1)-(3) it can be seen that ξ, z_2 and z_3 depend only on ρ; then, for a given value of ρ, z_3 is constant. This means

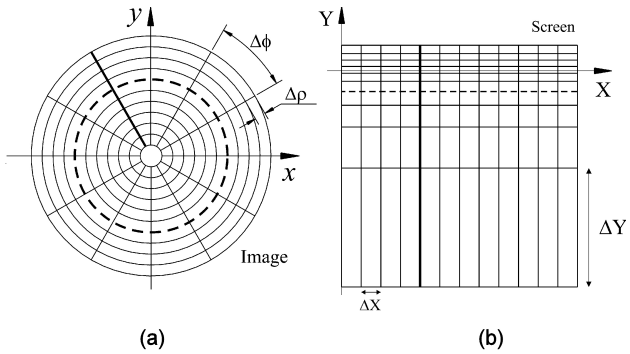

FIGURE 10. (a) On the image, circumferences centered at the origin and straight lines with equations ϕ = const are transformed, on screen (b), into horizontal and vertical lines, respectively.

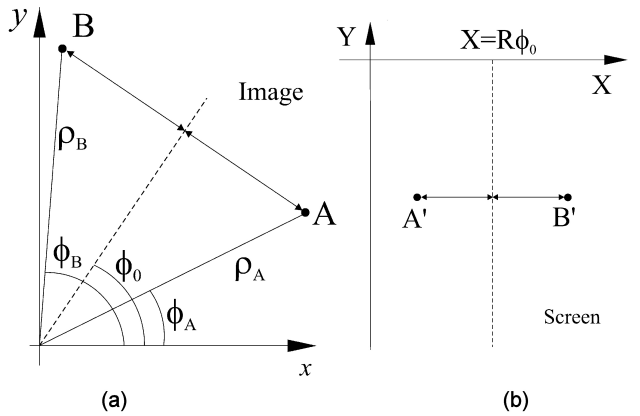

FIGURE 11. (a) On the image, symmetric points with respect to straight lines with equations ϕ = *const*; on the screen (b), are symmetric with respect to the vertical line *X = Rϕ*.

that a circumference centered at the origin of the image that is described by ρ = const (Fig. 10a) is transformed into a circumference on the cylinder described by z_3 = const. On the plane screen, this is a horizontal line with equation Y = const, as is shown by the dark dashed line in Fig. 10b.

In addition, from Eq. (5) it can be seen that straight lines on the CCD with equations ϕ = const are transformed on the cylinder and on the plane screen into vertical lines. In Fig. 10, one of this type of line is indicated with a continuous dark line.

Now, two points symmetrically located with respect to a straight line passing through the origin of coordinates at the image is transformed into a similar symmetric object on the plane screen. In order to show this, points $A$and B of the image are shown in Fig. 11a. They have coordinates (ρ_A, ϕ_A) and (ρ_B, ϕ_B) respectively, and are symmetrically located with respect to the straight line $\phi = \phi_0$; $i.e.$ $\phi_A = \phi_0 - \alpha, \phi_B = \phi_0 + \alpha$ and $\rho_A = \rho_B$. After applying the transformation, their corresponding points A' and B' on the screen (Fig. 11b) have, coordinates A' $(X_{A'}, Y_{A'})$ and B' $(X_{B'}, Y_{B'})$ respectively, in rectangular coordinates. They satisfy the following relationships: $X_{A'} = R(\phi_0 - \alpha)$, $X_{B'} = R(\phi_0 + \alpha)$, $Y_{A'} = Y_{B'}$, since Y depends only on ρ, and the straight line $\phi = \phi_0$ is transformed into the vertical straight line X = Rϕ_0. Then A' and B' are symmetrically located with respect to the vertical straight line X = Rϕ_0.

When the object and its image are symmetric, it is said that the symmetry is conserved. So, the last paragraph means that the transformation defined by Eqs. (5) and (6) maintains the symmetry with respect to straight lines on the image with equations ϕ = *const.* This fact is better illustrated in Fig. 12.

Examples of symmetric curves with respect to a straight line passing through the origin of coordinates are shown in Figs.12a and b. The first is a set of four squares where each one is symmetric with respect to a straight line of the form ϕ = const The second image is a pair of words "yes" symmetrically located in reference to a straight line passing through the origin of coordinates. The curves in Figs. 12c and d are their respective objects on the screen. As can be seen, in both cases the curves on the plane screen are symmetrical with respect to vertical straight lines. In each figure, the axes of symmetry, on the screen and on the image, are indicated with dotted lines.

As an example of where symmetry is lost, the same Fig. 12b is slightly displaced along the y-axis to obtain Fig. 13a. Even though the words "yes" on the image are symmetrically located with respect to a straight line, the curves on the screen in Fig. 13b not are symmetrical. This is because the axis of symmetry on the image is not of the form ϕ = *const*. In this case, it is said that the symmetry was lost. It is worth recognizing here that the loss of symmetry is not merely a scale change; it is not possible to resize one of the "yes" objects in Fig. 13b and to flip it horizontally to bring it in coincidence with the other "yes" object.

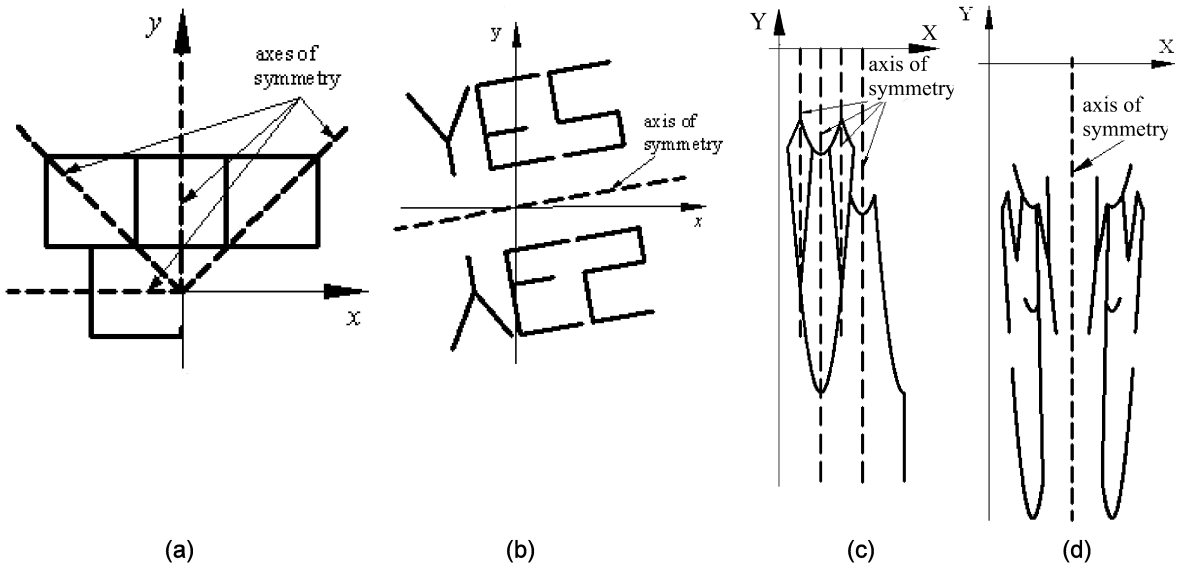

FIGURE 12. (a) and (b). Symmetrical images with respect to straight lines of the form ϕ = const. (c) and (d). On the screen, after applying the transformation symmetrical curves are obtained.

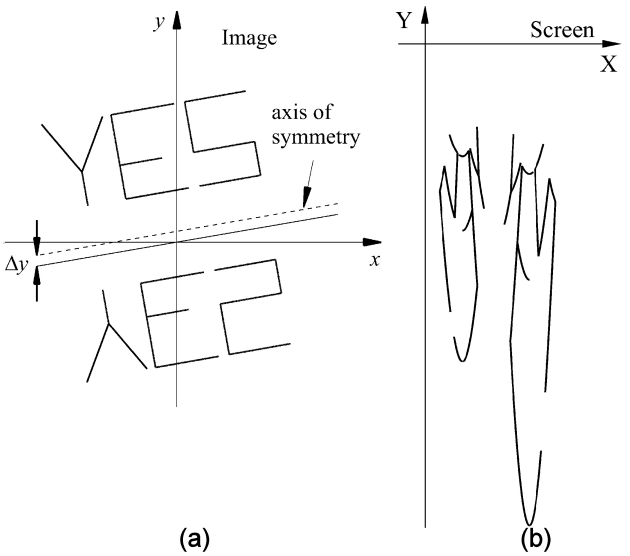

FIGURE 13. (a) The axis of symmetry on the image is not of the form ϕ = const. (b). The curves on the screen are not symmetrical.

The conservation of symmetry with respect to straight lines on the image with equation ϕ = const is not only valid [1] for spherical surfaces as reflecting optics, but it is true also for any surface of revolution centered on the Z-axis.

6. Conclusions

In this paper, a detailed analysis of the geometric aspects of the transformation from the image plane to the screen plane in null screen tests has been performed.

The main results of this analysis are:

1. For similar geometrical figures on the image, the corresponding objects on the screen can have remarkably different shapes. This is because the radial and azimuthal magnifications are very different. The azimuthal magnification is a linear function of ρ, while the mathematical expression for the radial magnification is a more complicated function which implicitly depends on ρ.
2. For a perfect circle on the image, its corresponding object on the screen has the following properties. The relative position between the point C' (the object point associated with the center C of the circle on the image) and the point M' (the geometric center of the corresponding *drop* shape on the screen) is in different positions depending on the position of the *drop* in the vertical direction. The relative position depends on whether the circle is in the region where the radial magnification is increasing or decreasing. In the first case, considering the vertical direction, the point C' is below the point M', while in the second case, the point C' is above M'.
3. It was noticed that, on the image, curves symmetric with respect to straight lines with equations ϕ = *const*, on the plane screen, are obtained from objects which are symmetric with respect to straight lines with equations *X* = *const*.
4. Looking at the pairs image-screen shown in this paper, it can be seen that, if the image has a uniform line density, on the screen the line density varies. This fact has an implication for the way a screen must be illuminated in order to obtain a uniformly illuminated image.

All these results are important facts that must be considered during the design of null screens for optical testing. Indeed, some of them have been used in several other papers, such as [9-11]. In particular, in Ref. 3, it is shown that in order to properly test optical surfaces with a null screen, the particular characteristic of the transformation described in point 3 must be taken into account to evaluate the centroids of the circular spot images.

Acknowledgements

The authors of this paper are indebted to Neil Bruce for his help in revising the manuscript. This research was supported by the Consejo Nacional de Ciencia y Tecnología (CONACyT), México, under Project No. U51114-F and by DGAPA-project PAPIIT No. ES-114507.

1. R. Díaz-Uribe and M. Campos-García, *Appl. Opt.* **39** (2000) 2670.
2. M. Campos-García, R. Díaz-Uribe, and F. Granados-Agustín, *Appl. Opt.* **43** (2004) 6255.
3. L. Carmona-Paredes. "Imágenes de aberturas elípticas en la prueba de superficies convexas con pantallas nulas". Master thesis on Physics. Universidad Nacional Autónoma de México, México (2005).
4. Y. Mejía-Barbosa and D. Malacara-Hernández, *Appl. Opt.* **40** (2001) 5778.
5. Sharon S. Welch, "Effects on Window Size and Shape on Accuracy Subpixel Centroid Estimation of Target Image." NASA Technical Paper 3331. September 1993.
6. B.F. Alexander and Kim Chew, *Opt. Eng.* **30(9)** (1991) 1320.
7. J. Ares and J. Arines, *Appl. Opt.* **43** (2004) 5796.
8. J.S. Morgan, D.C. Slater, J.G. Timothy, and E.B. Jenkins, *Appl. Opt.* **28** (1989) 1178.
9. M. Avendaño-Alejo, M. Campos-García, and R. Díaz-Uribe, "Tilted null screens with drop shaped spots: radial and square arrays," in *Frontiers in Optics, Laser Science, Optical Fabrica-*

tion and Testing and Organic Photonics and Electronics 2006 (Optical Society of America, Washington, DC, 2006), OFMC9.

10. V.I. Moreno-Oliva, M. Campos-García, and R. Bolado-Gómez, "Point-Shifting in the Optical Testing of Fast Aspheric Concave Surfaces by a Cylindrical Screen" (submitted to *Applied Optics*; 28 August, 2007).

11. R. Bolado-Gómez and M. Campos-García, "Testing Fast Aspheric Concave Surfaces with a Cylindrical Screen" (submitted to *Applied Optics*; 9, September, 2007)